GIScience & Remote Sensing

ISSN: (Print) (Online) Journal homepage: www.tandfonline.com/journals/tgrs20

Unmixing marsh vegetation species across multiple sensors and spatial scales

Zhicheng Yang, Tegan Blount, Conner Lester, Nat Blackford, Andrea D'Alpaos, Marco Marani, Brad Murray & Sonia Silvestri

To cite this article: Zhicheng Yang, Tegan Blount, Conner Lester, Nat Blackford, Andrea D'Alpaos, Marco Marani, Brad Murray & Sonia Silvestri (2025) Unmixing marsh vegetation species across multiple sensors and spatial scales, GIScience & Remote Sensing, 62:1, 2481689, DOI: 10.1080/15481603.2025.2481689

To link to this article: https://doi.org/10.1080/15481603.2025.2481689

GISCIENCE & REMOTE SENSING
2025, VOL. 62, NO. 1, 2481689
https://doi.org/10.1080/15481603.2025.2481689

Taylor & Francis
Taylor & Francis Group

Unmixing marsh vegetation species across multiple sensors and spatial scales

Zhicheng Yang [a], Tegan Blount [b], Conner Lester [a], Nat Blackford [a], Andrea D'Alpaos [b], Marco Marani [c], Brad Murray [a] and Sonia Silvestri [d]

[a]Division of Earth and Ocean Sciences, Nicholas School of the Environment, Duke University, Durham, NC, USA; [b]Department of Geosciences, University of Padova, Padova, Italy; [c]Department of ICEA, University of Padova, Padova, Italy; [d]Department of Biological, Geological, and Environmental Sciences, University of Bologna, Ravenna, Italy

ABSTRACT

Coastal marsh ecosystems are critical for providing essential habitats, buffering coastlines against erosion, and sequestering carbon. However, there is a global trend where these ecosystems are disappearing due to rising sea levels, wave-drive erosion, and human activities. Accurate and repeatable observations of marsh vegetation distributions are essential for understanding marsh resilience and informing conservation strategies. Mapping the fractional abundance (FA) of each marsh species using standard airborne/satellite sensor pixels can provide accurate information about marsh vegetation distribution and a deeper insight into marsh dynamics. This study explores the feasibility of estimating FA for marsh vegetation species across the diverse pixel sizes of different remote sensors, based on ground truthing information obtained from Unmanned Aerial Vehicle (UAV) data and field surveys. Specifically, the FA values of each species within the pixels from airborne, WorldView-2 (WV2), and Sentinel-2 (SL2) data, with pixel sizes of 0.15 m, 0.5 m, and 10 m, respectively, were estimated by using a Rescaled Random Forest Regression (RRFR) algorithm. Our results suggest that Random Forest Classification can accurately classify marsh vegetation, with extremely high levels of accuracy when applied to UAV data. This demonstrates that UAVs are cost-effective and efficient for acquiring ground truthing to inform FA estimation algorithms. Our analyses also indicate that the RRFR can accurately unmix dominant marsh species (*Spartina* and *Juncus*), as well as bare soil, across various spatial resolutions. However, the unmixing of *Salicornia*, a minor species, proved to be challenging, indicating the need for additional ground truthing data to capture information relating to minor species. The approach proposed in this study can facilitate the analysis and monitoring of marsh vegetation dynamics, supporting effective conservation and management practices to enhance marsh resilience.

ARTICLE HISTORY
Received 18 September 2024
Accepted 15 March 2025

KEYWORDS
Coastal marsh; UAV; airborne data; satellite data; unmixing

Introduction

Coastal marshes are critical ecosystems, providing essential habitats for numerous species, buffering coastlines against erosion, and sequestering carbon (e.g. Barbier et al. 2011). However, these ecosystems are disappearing at a global scale (e.g. Blum and Roberts 2009; Carniello, Defina, and D'Alpaos 2009; Horton et al. 2018), due to reduced sediment transport to coastal areas, land use changes, sea level rise, wave-driven erosion, and human activities (e.g. Allen 2000; Marani et al. 2011; Möller et al. 2014; Tognin et al. 2021).

Marsh vegetation plays a critical role in supporting marsh resilience through multiple mechanisms. By trapping sediment and reducing water flow, vegetation promotes sediment deposition and stabilizes the marsh surface, enhancing its resistance to erosion. Additionally, the production of biomass, particularly belowground biomass, contributes significantly to marsh accretion, enabling the marsh to maintain its elevation relative to sea level. These processes are essential for the long-term survival and stability of marsh ecosystems, especially in the face of rising sea levels and climate change (e.g. Bouma et al. 2007; D'Alpaos, Mudd, and Carniello 2011; Marani et al. 2010, 2007; Morris et al. 2002; Murray et al. 2008; Zong and Nepf 2010). Marsh vegetation often forms distinct patches with varying densities of typical species interspersed with bare soil areas or with the mixture of different species (e.g. Da Lio, D'Alpaos, and Marani 2013; Marani, Da Lio, and D'Alpaos 2013;

CONTACT Zhicheng Yang yang-thinkmore@outlook.com
Supplemental data for this article can be accessed online at https://doi.org/10.1080/15481603.2025.2481689

Roner et al. 2016; Silvestri, Defina, and Marani 2005). Such zonation distribution patterns reflect vegetation adaptations to environmental stressors (e.g. edaphic conditions and hydrodynamic stresses), and interspecies interactions (e.g. inter-specific competition and facilitation) (e.g. Da Lio, D'Alpaos, and Marani 2013; Finotello et al. 2022; Marani, Da Lio, and D'Alpaos 2013, Marani et al. 2006; Pennings, Grant, and Bertness 2005; Silvestri, Defina, and Marani 2005). Variations in sea level (e.g. Morris et al. 2002), the occurrence of drought (Alber et al. 2008; Yang et al. 2025) and storms (Howes et al. 2010), geomorphological processes (e.g. D'Alpaos et al. 2005; Yang, Alexander, and Alber 2024), as well as animal and human activities, can alter vegetation distribution (e.g. Deegan et al. 2012; Silliman et al. 2005). These are displayed as inter-specific replacements, vegetation mortality, and possible recovery processes, which are of great importance to marsh survival, biodiversity, and ecosystem services.

Given the critical role of marsh vegetation in promoting marsh accretion to possibly match the rate of sea level rise, accurate and repeatable observations of its distribution are essential. To characterize the entire ecosystem, these observations are required to cover a wide range of scales, both in space (from centimeters to tens of kilometers) and time (days to decades). Remote Sensing (RS) is a promising tool to undertake this task. Previous analyses have primarily relied on hard classification of vegetation species presence, which assigns each pixel or pixel group (i.e. object) to a single species or community (e.g. Belluco et al. 2006; Campbell et al. 2017; Juel et al. 2015; Timm and McGarigal 2012; Van Beijma, Comber, and Lamb 2014). The accuracy of hard classifications can be improved by integrating the spectral information with co-occurrence matrices, which analyzes image texture by examining the spatial relationships between pixels (Lane et al. 2014). However, these approaches cannot capture the sub-pixel variability in species composition. The sensors commonly used for monitoring marshes have spatial resolutions ranging from about half a meter to tens of meters. Given the typical size and spatial distribution of species in many marshes, pixels tend to display mixtures of different vegetation species and bare soil (see sample nadir-looking photographs in Figure 1).

The number of studies focusing on unmixing marsh vegetation species or on estimating Fractional Abundance (FA, i.e. the relative area occupied by a given species when observed from above) of each species is limited (e.g. Silvestri, Marani, and Marani 2003; Wang et al. 2007; Yang et al. 2020). Progress in the use of RS data to accurately capture the fine-scale spatial distribution of vegetation species would greatly increase our understanding of the relevant ecological processes. Accurate marsh species maps enable the identification of the most vulnerable areas (Ganju et al. 2017, 2022), thus enhancing data-driven conservation strategies and optimizing marsh management practices. In addition, FA values were required by numerous marsh evolution modeling to study species competition and understand system evolution (e.g. Finotello et al. 2022; Marani et al. 2006; Marani, Da Lio, and D'Alpaos 2013; Roner et al. 2016). Therefore, accurate estimates of FA are important to improve our ability to predict marsh destiny under changing climatic and environmental conditions.

Previous studies estimating the FA of marsh species have relied heavily on artificial neural networks (ANNs, Wang et al. 2007). While ANNs can achieve high accuracy, they require a time-consuming training phase, their performance being very sensitive to the choice of their structure. This complexity makes the implementation and optimization of an ANN for marsh FA estimation a challenging task. Another limitation of existing approaches to estimating marsh FA is their dependence on specific choices of vegetation indices, used to separate vegetated and bare soil areas (Ganju et al. 2022; Zhou, Yang, and Chen 2018). Such indices, however, are sensitive to species-specific reflectance patterns, such that the available spectral information is not fully utilized, and the resulting effectiveness is consequently limited. These limitations highlight the need for more efficient and robust methods for estimating marsh species FA.

Machine learning algorithms have proven effective in estimating the FA of various land cover types
(L. Yang et al. 2017), including shrub communities (Schwieder et al. 2014), grassland (Chai et al. 2019), habitats on coastal dunes (Pafumi et al. 2025), forest species (Immitzer et al. 2018) and coastal habitats (Martínez Prentice et al. 2024). Machine learning-derived FA estimates have been used to model the probability of co-occurrence between

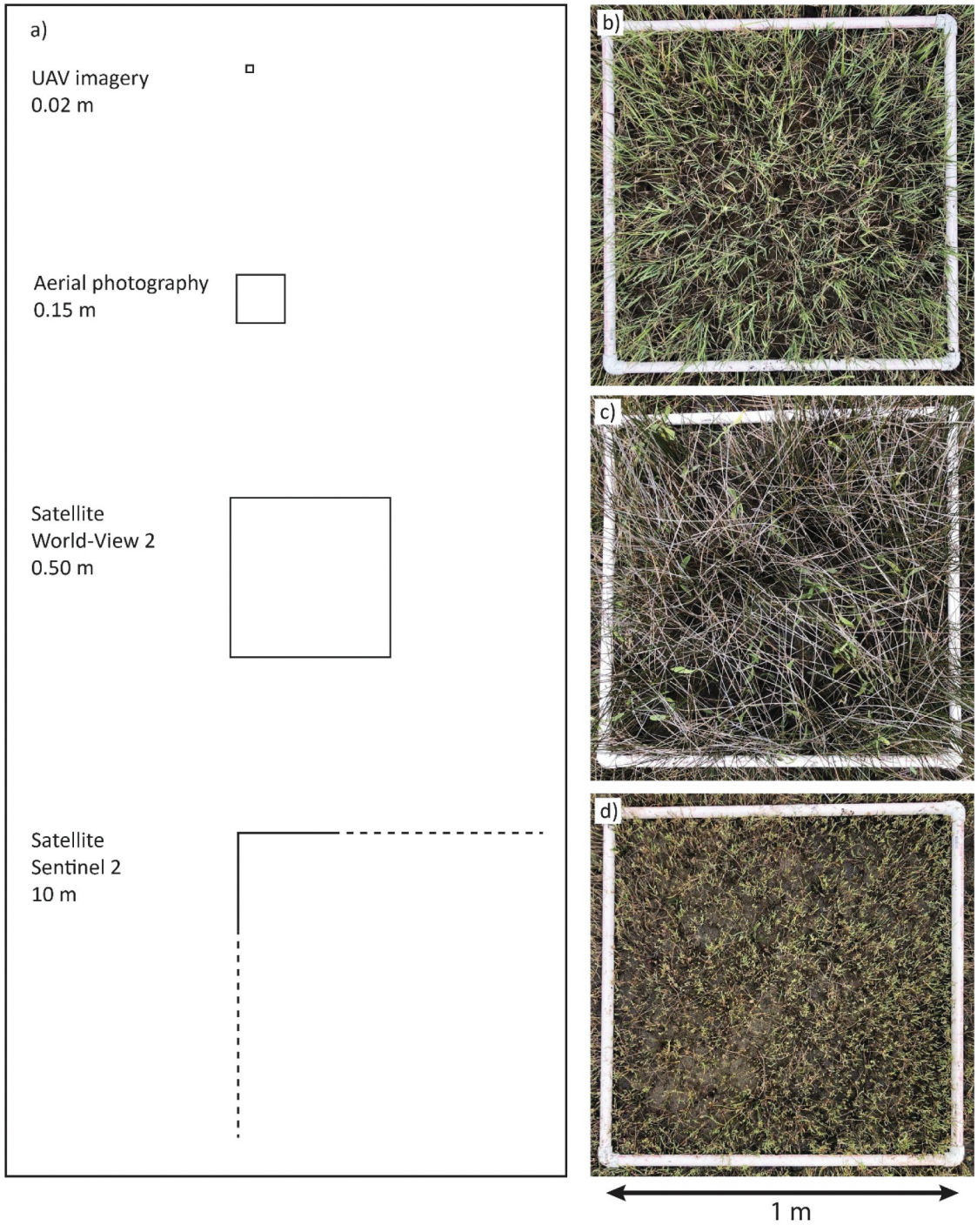

Figure 1. Comparison of typical remote-sensing sensors and photos taken from vegetation plots. Panel (a) Shows the spatial resolution of different remote-sensing sensors. Panels (b-d) show photos taken from plots of main species occupying marshes within North Inlet-Winyah Bay National Estuarine Research Reserve, i.e. *Spartina alterniflora* (b), *Juncus roemerianus* (c), and *Salicornia virginica* (d), respectively.

paired land cover types (Costa, Foody, and Boyd 2017; Pafumi et al. 2025; Xu et al. 2005; Yang et al. 2020), leading to improvements in classification accuracy. This type of applications suggests the potential of machine learning algorithms to map marsh species FA to obtain similarly accurate information for marsh monitoring at both local and large scales

Traditional FA estimation requires extensive field surveys to comprehensively record species mixtures

across the entire marsh (Yang et al. 2020), which are resource-intensive and labor-consuming. An alternative approach lies in Unmanned Aerial Vehicles (UAVs) equipped with extremely high-resolution multispectral sensors, offering a more cost-effective solution with resolutions typically ranging from 0.01 to 0.50 m (Dai et al. 2021; Doughty and Cavanaugh 2019; Morgan et al. 2022; Yang, Alexander, and Alber 2024). The primary advantage of such high spatial resolution is that the majority of pixels can capture the reflectance of individual species rather than that of a mixture of species, as demonstrated in Figure 1 and some existing observations (e.g. Lynn et al. 2023; Yang, Alexander, and Alber 2024). The application of hard classifiers in this case can be highly accurate as the pixel size is smaller than the typical scale of variability in species (bare soil) composition. UAV-borne sensors, however, cannot easily acquire data over very large areas, due to typical operational constraint, such as battery capacity, tidal flooding of the study area, and regulatory constraints. Hence, the potential of high-resolution UAV multi-spectral data for FA estimation remains largely unexplored (Martínez Prentice et al. 2024).

This study aims to test the hypothesis that high-resolution UAV data can be effectively used to provide ground truthing information for estimating marsh species FA across different spatial resolutions, including airborne and satellite data. We specifically investigate 1) the feasibility of using UAV data for species unmixing, 2) the potential for estimating species FA within airborne and satellite data, and 3) the accuracy of our methods in providing percentage cover estimates for different marsh species across a range of spatial resolutions. The findings of this work have implications for the monitoring of marsh vegetation and its extent, particularly in the context of rising sea levels and climate changes, thus informing strategies for managing and preserving marsh ecosystems.

Methods

Study site

This analysis focused on marshes within the North Inlet-Winyah Bay National Estuarine Research Reserve (NIWB), South Carolina (SC, top-left panel of Figure 2). NIWB is formed by the convergence of the North Inlet Estuary and Winyah Bay Estuary, situated along the southeastern coast of the Atlantic Ocean. North Inlet is characterized as an ocean-influenced estuary. The North Inlet basin receives limited freshwater from Winyah Bay and adjacent upland runoff. In contrast, Winyah Bay is classified as a brackish water estuary primarily influenced by freshwater input from upstream rivers (Dame and Gardner 1993).

The water level in this area is chiefly determined by a semi-diurnal mixed tide, with an average range of about 1.5 m (Hughes, Wilson, and Morris 2012). This region has experienced a sea level rise trend of about 3.3 mm/yr between 1957 and 2023 (National Oceanic and Atmospheric Administration 2023). This trend estimate is based on tidal elevations recorded at the Springmaid Pier tidal gauge (Figure 2), which is the closest tidal gauge to the NIWB, located approximately 50 km away. The Springmaid Pier tidal gauge also provides tidal elevation data at the time of image acquisition in this study with reference to Mean Sea Level (MSL)

Within NIWB, marsh vegetation exhibits a zonation pattern characterized by distinct species dominance, with individual patches predominantly occupied by a single species and exposed to bare soil. Marshes within NIWB are primarily dominated by two types of marsh communities: a salt marsh community, dominated by *Spartina alterniflora*, and a brackish marsh community, mainly occupied by *Juncus roemerianus* (Li et al. 2022).

Spartina alterniflora (Figure 1b), commonly known as cordgrass (referred to as "*Spartina*" hereafter), dominates the salt marshes in the North Inlet estuary. It occupies depressed marsh areas with high salinity and long waterlogging period (see Figure 2). In contrast, *Juncus roemerianus* ("*Juncus*," Figure 1c) is typically found in low salinity zones near the marsh boundary with the upland (see Figure 2), while *Salicornia virginica* ("*Salicornia*," Figure 1d) tends to grow in the intermediate areas (see Figure 2) (Allen et al. 2008; Dame and Gardner 1993). This zonation pattern along salinity gradients is driven by ecological interactions, with *Spartina* occupying high-salinity environments due to its lower competitive ability in comparison to *Juncus* and *Salicornia* (Pennings, Grant, and Bertness 2005).

Marsh vegetation within NIWB has experienced multiple drought-related diebacks, potentially hindering its resilience to rising sea levels and climate change (Li et al. 2022). This highlights the importance of robust methods for accurately mapping and updating marsh vegetation FA to support effective marsh management.

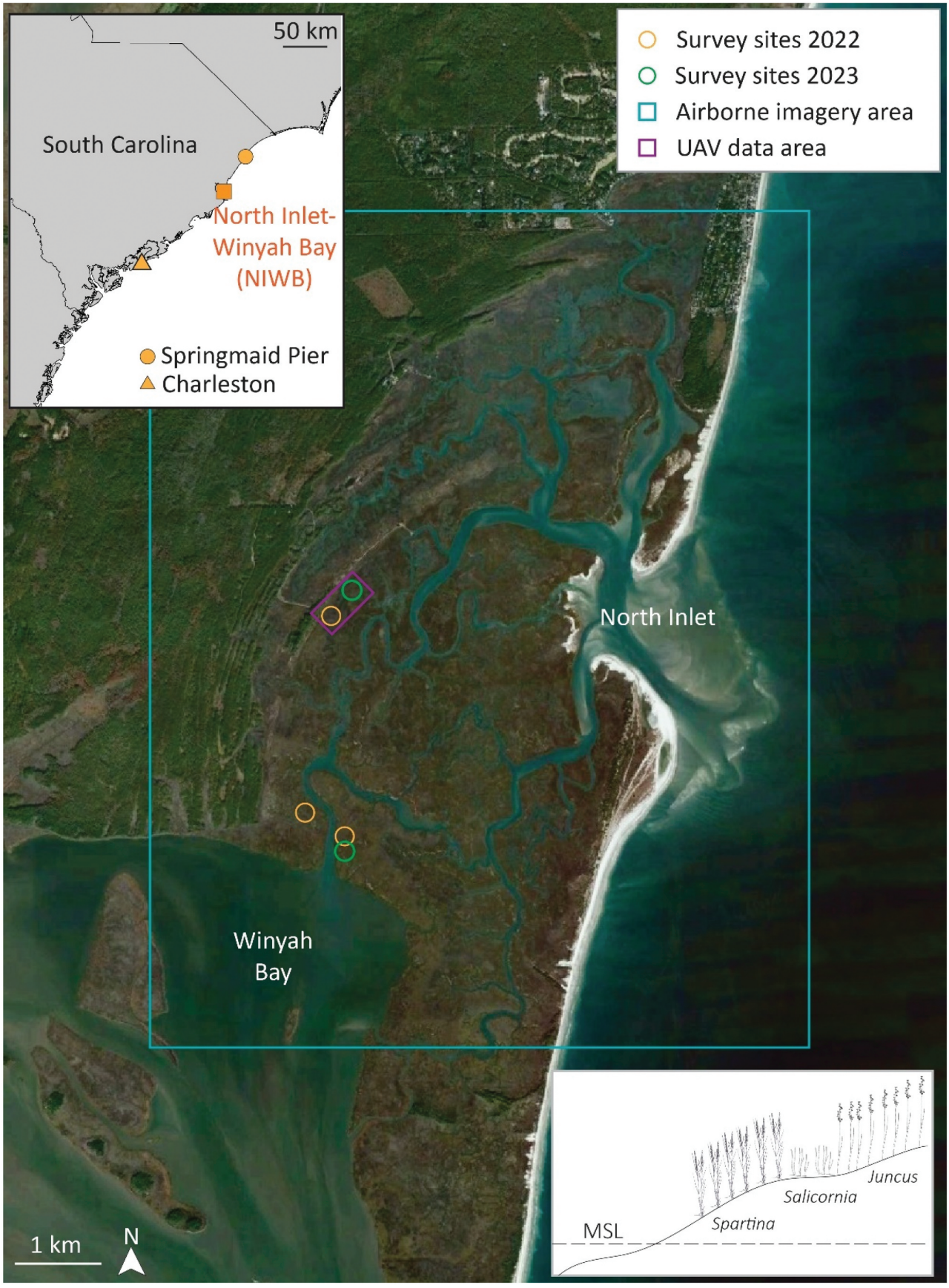

Figure 2. Overview of the research area. The inset in the top-left shows the southeastern coast of the USA and the location of the NIWB. The main map shows the aerial view of the NIWB marshes (image © 2024 CNES/Airbus). The positions of Springmaid Pier tidal gauge and meteorological station in Charleston are highlighted. It also displays the positions of field surveys conducted in the location of the NIWB in 2022 and 2023. The areas of UAV data collection and airborne data acquisition are also marked. The bottom-right panel illustrates the typical ecological gradient and distribution of marsh vegetation species. Please note that elevation and distance in the bottom-right panel are not to scale.

Image collection

UAV multispectral data

The UAV data were acquired within a targeted portion of the wider study area (Figure 2), using a DJI M300 UAV equipped with a Micasense Altum sensor and internal GPS. This sensor captures spectral information across the blue (centered: 475 nm, bandwidth: 32 nm), green (centered: 560 nm, bandwidth: 27 nm), red (centered: 668 nm, bandwidth: 14 nm), red-edge (centered: 717 nm, bandwidth: 12 nm) and near-infrared (centered: 842 nm, bandwidth: 57 nm) bands. Data collection occurred during low tide (−0.62 m above MSL) at 15:22 on 27 August 2023. The UAV acquired the data with a pixel resolution of about 0.02 m at an elevation of 40 m above the ground. Data acquisition was completed in two flights, each lasting about 35 min, maintaining a speed of 3.3 m/s. To ensure comprehensive coverage and precise data acquisition, the sensor acquired a scene every 1 s, with 70% side overlap and 75% front overlap.

Airborne multispectral data

The airborne remote sensing data were collected in the middle area of the NIWB (Figure 2). Data were captured on 6 October 2022, with sunny weather conditions and very little cloud cover. The aircraft was a fixed-wing Cessna 208B Caravan equipped with an UltraCam Eagle M3 camera. This sensor captured four spectral bands in the blue (380–590 nm), green (425–650 nm), red (575–700 nm), and near-infrared (670–1000 nm) part of the spectrum with a spatial resolution of 0.15 m.

WorldView-2 data

WorldView-2 (WV2), a commercial earth observation satellite operated by Maxar, operates a sensor capturing data through a high spatial resolution (0.5 m) Panchromatic band (447–808 nm) and eight multispectral bands with a lower resolution (2 m). These bands include coastal blue (396–458 nm), blue (442–515 nm), green (506–586 nm), yellow (554–632 nm), red (624–694 nm), red-edge (699–749 nm), near-infrared 1 (765–901 nm), and near-infrared 2 (856–1043 nm). The WV2 data used in this analysis was acquired in 16:18:43 on 8 September 2023, with a tidal level of about 0.37 m above the MSL.

Sentinel-2 data

The Sentinel-2 mission includes two Earth-observation satellites managed by the European Space Agency (ESA) as part of the Copernicus Programme. Equipped with the Multi-Spectral Instrument (MSI), Sentinel-2 satellites capture imagery in various spectral bands with a revisit period of about 5 days. The spatial resolution of Sentinel-2 data typically ranges from 10 to 60 m, depending on the spectral band.

In this study, we utilized Sentinel-2 Level 2A (SL2) product, which provides atmospherically corrected surface reflectance values. Our focus was estimating the FA of different species. We thus primarily utilized SL2 spectral bands spanning from visible to near-infrared bands, as they provide useful information about vegetation density and biomass. This preference primarily stems from two main reasons: i) vegetation exhibits strong absorption in the visible spectral range, mainly in the blue and red, due to high chlorophyll absorption; ii) vegetation also displays a significant increase in reflectance in the near-infrared spectrum portion, due to the scattering of near-infrared radiation within the internal leaf structure (Gates et al. 1965). These bands include blue (459–479 nm), green (541–558 nm), red (655–680 nm), red-edge 1 (697–712), red-edge 2 (732–747 nm), red-edge 3 (773–793 nm), near-infrared (784–-899 nm), and red-edge 4 (855–875 nm).

Fieldwork

To provide ground truthing information for image classification and FA estimation, we conducted field measurements in August 2022 and August 2023 (Figure 2). In each survey, we employed a stratified random sampling approach to select a series of 1×1 m quadrats. We first identified zones dominated by *Spartina*, *Juncus*, or *Salicornia* and then randomly selected quadrats within each zone. This ensured the inclusion of a wide range of species compositions and vegetation densities within our sample set and avoided any unconscious selection bias by the field operator. The positions of the corner points of each quadrat were recorded using an Emlid Reach RS2 Real-Time Kinematic (RTK) GNSS receiver operating in the NAD83 (2011)/South Carolina coordinate system. Within each quadrat, we recorded the species present and the FA of each species, estimated by the

standard Braun–Blanquet method (e.g. see Belluco et al. 2006). The quadrats were surveyed in 2022 and 2023, reaching a total of 26 and 22 quadrats, respectively.

In addition to the marsh vegetation plots, we selected some marsh portions occupied by soil and wrack, based on the RGB composition of the UAV imagery. These were also used in the UAV image classification process. It is worth noting that wrack burial areas and bare soil were considered bare land cover in this study, primarily because wrack tends to kill most of the buried vegetation (Pennings and Richards 1998).

Data preprocessing

UAV data

The overlap parameters in the data acquisition phase ensured that each tile adequately covered neighboring tiles. This allowed us to perform georectification, orthorectification, and radiometric correction using bundle block adjustment in the Pixel-4D software. This software employs bundle block adjustment, a photogrammetric technique that simultaneously refines the camera position and orientation parameters for each image in a dataset, along with the 3D coordinates of ground control points (GCPs) (Yuan 2009). As the UAV sensor's internal GPS was not connected to the RTK system, precise georeferencing was achieved in the post-collection-processing phase using GCPs. To achieve this, we deployed a series of GCPs across the study area. These GCPs were surveyed using an Emlid RS2 GNSS receiver, connected to a North Carolina Continuously Operating Reference Station (CORS) network station (NCSL) approximately 100 km away. This setup ensured a horizontal accuracy of ±1 cm, contributing to the precise georeferencing of the UAV data. The accuracy of the georectification and orthorectification process was assessed by calculating the root-mean-square error (RMSE) between the measured image coordinates of the GCPs and their corresponding ground coordinates. This produced data of high spatial accuracy, with an average RMSE of about 0.05 m. Furthermore, the UAV data also encompassed some upland forests and human-paved roads (Figure 3a). These areas were manually identified and digitized and subsequently excluded from the following classification processes.

WV2 data

We applied atmospheric correction to the multispectral bands of the WV2 data to obtain an accurate spectral reflectance. For this purpose, we used the Fast Line-of-sight Atmospheric Analysis of Spectral Hypercubes (FLAASH) algorithm (Cooley et al. 2002). The main steps are outlined in Supporting Information.

Our primary focus was to estimate the FA of each marsh species, and the presence of channel networks and tidal forests had the potential to cause some errors. To minimize that, we manually digitized these features based on visual observations of the RGB composition of the WV2 data and excluded them from the following FA estimation process.

Airborne multispectral data

When we overlaid the UAV data, airborne data, and WV2 data, we observed that the position of the road in the UAV data was consistent with that in WV2 data. However, there were some inconsistencies when compared with its location in the airborne data. Therefore, georectification of airborne data was necessary. Specifically, since the airborne data covers an area of approximately 50 km^2, we selected 18 points assumed to have consistent positions between 2022 and 2023. These points were located at marinas, buildings, boundaries between forests and marshes, and branch points of small channels in the overlapping area of the airborne and WV2 data. Georectification with affine transformation was then performed on ArcGIS 10.8 using these reference points, and georectification resulted in an average RMSE of 0.41 m.

To enable accurate FA estimation from airborne mosaic data, we converted the 8-bit Digital Numbers (DN) of georectified airborne data to reflectance values, using the WV2 reflectance data as a reference. This procedure is similar to the procedure utilized by Oostdijk et al. (2018), which is described in detail in Supporting Information.

Sentinel-2 data

The SL2 blue, green, red, and near-infrared bands have a spatial resolution of 10 m, while the SL2 red-edge bands have a resolution of 20 m. To fully use the information from the SL2 red edge bands, we considered the average reflectance values of the blue, green, red, and near-infrared bands as

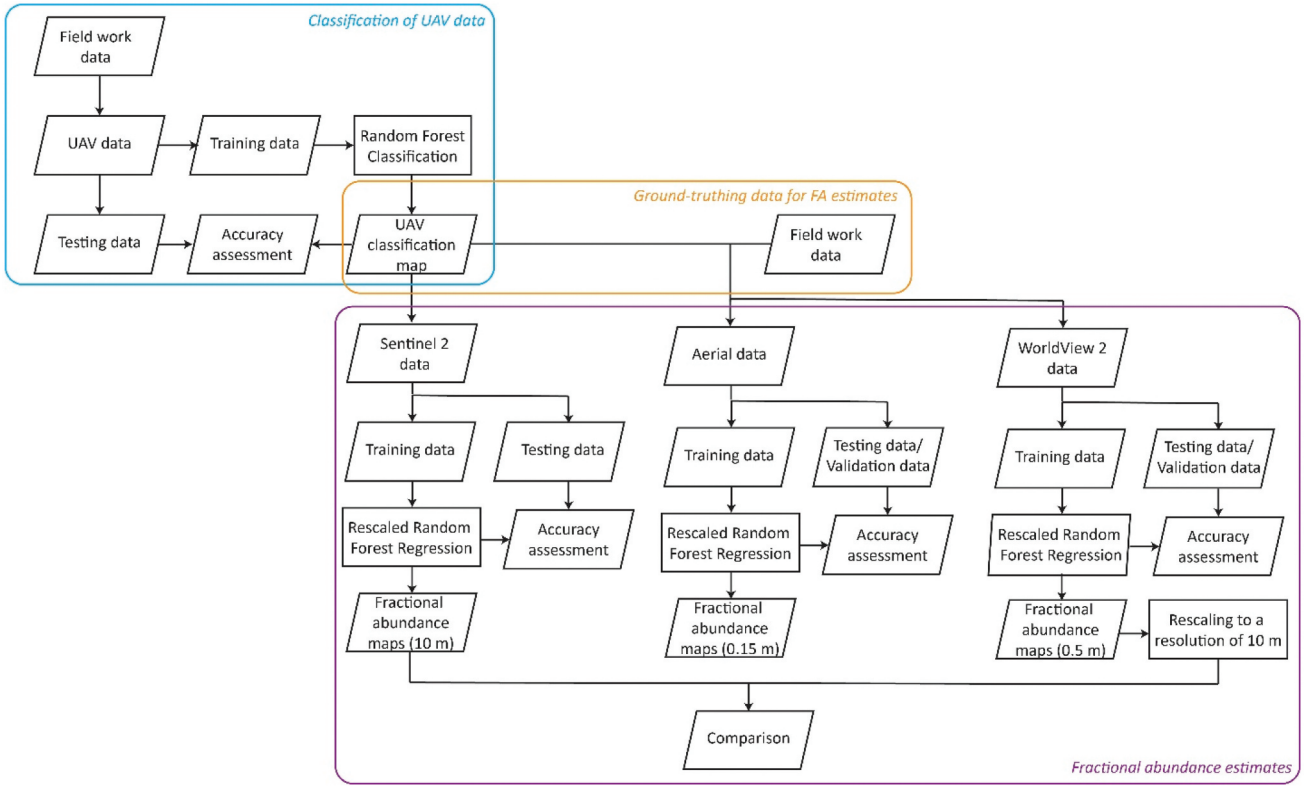

Figure 3. The workflow of the present study.

the panchromatic band and pan-sharpened all SL2 red edge bands to a spatial resolution of 10 m using the Gram-Schmidt Pan Sharpening algorithm. This approach, utilizing average values of the remaining visible to near-infrared bands as the panchromatic band and the Gram-Schmidt Pan Sharpening algorithm has been validated as a reliable method for pan-sharpening SL2 red edge bands (Kaplan 2018).

Then, SL2 pixels with low levels of quality resulting from cloud cover and shadows were filtered out using the quality assessment band (Copernicus 2024). Additionally, to address the potential reduction in reflectance within the near-infrared band due to marsh platform submergence and to facilitate future multi-year analyses of vegetation changes, we used average reflectance values for each band across the vegetation growing season (June to September) in 2023, instead of SL2 data from a single date. The pan-sharpening of the SL2 red-edge bands, pixel filtering, and reflectance averaging were conducted using Google Earth Engine.

Classification of the UAV data

Our primary objective in this study was to accurately estimate FA of vegetation species and bare soil. The main workflow of this study is shown in Figure 3. To provide accurate information for FA estimation, we chose to preserve the scattered bare soil areas between plant stems in the UAV data classification. This led us to select pixel-based classification over object-based methods, even though the latter are common in high-spatial resolution data analysis and often produce smoother and more homogenous classification results (e.g. Costa, Foody, and Boyd 2017; Juel et al. 2015; Moffett and Gorelick 2013). The classification of the UAV data was accomplished using the Random Forest Classification (RFC) algorithm (Breiman 2001), because it had been successfully used for vegetation species classification in different landscapes (Belgiu and Drăgu 2016; Yang et al. 2020). RFC offers several advantages, including its ability to effectively manage a large number of input bands, mitigate data dimensionality issues, and reduce the risk of overfitting (e.g. Belgiu and Drăgu 2016).

To establish the dataset for UAV data classification, quadrats within the UAV acquisition area surveyed in 2023 (Figure 2a) and six digitized bare marsh portions (with a total area of about 1 m^2) were utilized. In particular, all pixels falling within these bare areas were used to provide spectral information about the bare land cover to the classifier. For the field-surveyed quadrats, we applied a pixel filtering process to ensure that only pure pixels representing the target vegetation were included. This involved visually inspecting the imagery and identifying and excluding pixels that fell on soil due to gaps in vegetation. The remaining pure pixels, fully covered by the target vegetation, were used to provide spectral information of each species to the RFC. A total of 29,464 pixels were used for RFC construction, 75% ($n = 22{,}098$) of them for training and the remaining 25% ($n = 7{,}366$) for testing the accuracy of RFC.

The map produced with this method was then used to calculate the FA of each species or bare class using airborne, WV2, and SL2 data, as described below.

FA estimates within airborne, WV2, and SL2 pixels

The FA estimation was conducted using the Random Forest Regression (RFR) algorithm. RFR is similar to RFC but considers the target (i.e. FA) as continuous numeric data, establishing a non-linear relationship between the input variables (i.e. spectral information) and the target (i.e. FA of each species or bare soil, see Figure S2). Therefore, RFR shares the same advantages as RFC. RFR has been widely utilized to estimate the relative cover of communities and tree species within coastal landscapes and forests (e.g. Immitzer et al. 2018; Martínez Prentice et al. 2024). For a detailed description of RFC and RFR, please refer to Breiman (2001).

Species-specific RFR models were built individually for airborne, WV2, and SL2 data, with each RFR comprising 500 regression trees. Subsequently, FA of each species was estimated by adjusting the RFR-predicted values of all species and exposed soil in the same pixel to collectively sum to 100% (Immitzer et al. 2018; Yang et al. 2020). This algorithm is henceforth referred to as Rescaled Random Forest Regression (RRFR) in subsequent discussions.

FA estimation for airborne data

To train and validate the RRFR, we used Regions of Interest (ROIs) generated both within the map produced using UAV data and field-surveyed plots. As mentioned above, the georectified multispectral data have an average RMSE of 0.41 m, which is larger than the pixel size of the airborne data. To avoid potential pixel misalignment between airborne and UAV data, we have selected ROIs based on homogeneous or heterogeneous vegetation/soil patches rather than individual pixels. By ensuring that each ROI covered a relatively large area of approximately 50 m^2 – sufficient to encompass 18 airborne and 350 UAV pixels – we minimize the impact of potential misalignment. Within the UAV-mapped area (Figure 2), we randomly digitized a total of 32 patches to serve as ROIs, ensuring no overlap and avoiding any subjective selection bias by excluding visual interpretation of the imagery. Out of these, we randomly selected 20 ROIs, together with 13 quadrats randomly chosen out of the total 26 quadrats surveyed in 2022, composed of a total of 49,045 pixels (the distribution of pixels within the ROI was described in the Supporting Information and Figure S3) used for training and testing the RRFR. Specifically, 36,783 pixels (75%) were randomly selected to train the model, and the remaining 12,262 pixels (25%) were used to test its accuracy. Additionally, the remaining 12 ROIs and the remaining 13 quadrats were used as an independent validation dataset, to further assess the model's accuracy. It is worth noting that estimating FA within airborne pixels using RFC classification results was based on the assumption that the vegetation density remained relatively consistent between 2022 and 2023.

FA estimation for WV2 data

For FA estimates within WV2 pixels, we followed a similar approach to that used for airborne photographs, but substituted the quadrats surveyed in 2022 with those measured in 2023 (Figure 2). Due to the larger pixel size of WV2 compared to airborne data, fewer pixels, i.e. 3419, 1140, and 1843 pixels, were used to train, test, and validate the RRFR applied to WV2 data.

FA estimation for SL2 data

SL2, which has larger pixels when compared to airborne and WV2 data, comprised 1451 pixels within the marsh portions acquired by the UAV. To ensure sufficient spectral information for the RRFR for SL2, all these pixels were utilized; therefore, no pixels were saved to perform additional validation. As in previous cases, these pixels were divided into two parts: 75% ($n = 1088$) for training and 25% ($n = 363$) for testing the accuracy.

Unlike the approaches applied with airborne and WV2 data, field-measured quadrats were not used to inform the RRFR for SL2. This decision was primarily due to the fact that vegetation appearance in quadrats cannot accurately represent the true situation of the area falling within SL2 pixels, given the small size of quadrats (1 m^2) compared to SL2 pixels (100 m^2).

Both RFC and RRFR were implemented using the Scikit-learn package (Pedregosa et al. 2011), which is an open-source machine-learning framework designed for the Python programming language. Five hundred decision/regression trees were built in the training phases of RFC/RRFR without growth limitation. The remaining parameters were set at their default values in the Scikit-learn package (see Table S1 in Supporting Information and Pedregosa et al. 2011).

Accuracy assessment

The evaluation of RFC performance utilized the Confusion Matrix, providing metrics such as Overall Accuracy (A), which represents the ratio of correctly classified testing pixels to the total number of testing pixels, regardless of species (Foody 2002). Additionally, the Kappa coefficient (K) was employed to represent the proportion of correctly classified testing sites after accounting for random agreements (Rosenfield 1986). Furthermore, to quantify the accuracy of RRFR, metrics, such as RMSE and coefficient of determination (R^2), were calculated for each species (Chai and Draxler 2014; Kvålseth 1985). The estimation of RRFR performance was based on the comparison between predicted FA and test/validation values:

$$\mathrm{RMSE} = \sqrt{\frac{\sum_{i=1}^{n} (y_i - \hat{y}_i)^2}{n}} \quad (1)$$

$$R^2 = \frac{\sum_{i=1}^{n} (\hat{y}_i - \bar{y})^2}{\sum_{i=1}^{n} (y_i - \bar{y})^2} \quad (2)$$

where y_i is the ground referential value, $\hat{y}_i$ represents the predicted value, $\bar{y}$ is the average of the observed values, and n is the number of test pixels

Both the WV2 and SL2 data used in this study were acquired in 2023, presenting an opportunity to explore the performance of RRFR for SL2 pixels using results from WV2 data. Due to the difference in spatial resolutions between WV2 and SL2, we resampled the FA values derived from WV2 by averaging them to match the SL2 grids. Subsequently, we established a linear regression relationship without an intercept between these resampled values and the FA values in the SL2 pixels for each species. The slope and goodness of fit (r^2) were used to evaluate the consistency of FA values derived from WV2 and SL2 data. Comparing the SL2-derived FA with the rescaled WV2 FA, which has been validated with independent test and validation datasets, allows us to better estimate the accuracy of FA estimated by SL2, especially given the limited number of SL2 pixels and the lack of an independent validation dataset for this coarser resolution. This cross-resolution comparison also helps evaluate the consistency of FA estimates derived from different spatial resolutions and determine how well the RRFR model generalizes across scales. The resampling and regression processes were conducted in ArcGIS 10.8 and Origin 2018, respectively.

Results

UAV image classification

The application of the RFC algorithm to UAV data achieved a high level of accuracy in classifying marsh vegetation species. The confusion matrix (Table 1) shows that $A = 0.99$ and $K = 0.98$. Specifically, 99.6%, 98.7%, 99.6%, and 98.8% of *Juncus*, *Salicornia*, *Spartina,* and bare areas in the test dataset were accurately classified. These results indicate that the RFC can effectively discriminate different species and bare soil within the UAV imagery (see Figure 4 for the UAV data and the classification results).

Figure 5 displays the FA of each species or bare area in the airborne photograph (Figure 5a-d), WV2 (Figure 5e-h), and SL2 (Figure 5i-l) pixels, calculated based on the RFC results of UAV data (Figure 4b). The

Table 1. Confusion matrix for UAV data classification by RFC.

	Test pixels				
Classes	*Juncus*	*Salicornia*	*Spartina*	*Bare*	*Total*
Juncus	1510	0	5	8	1523
Salicornia	2	447	4	0	453
Spartina	11	1	4271	6	4289
Bare	10	0	3	1088	1101

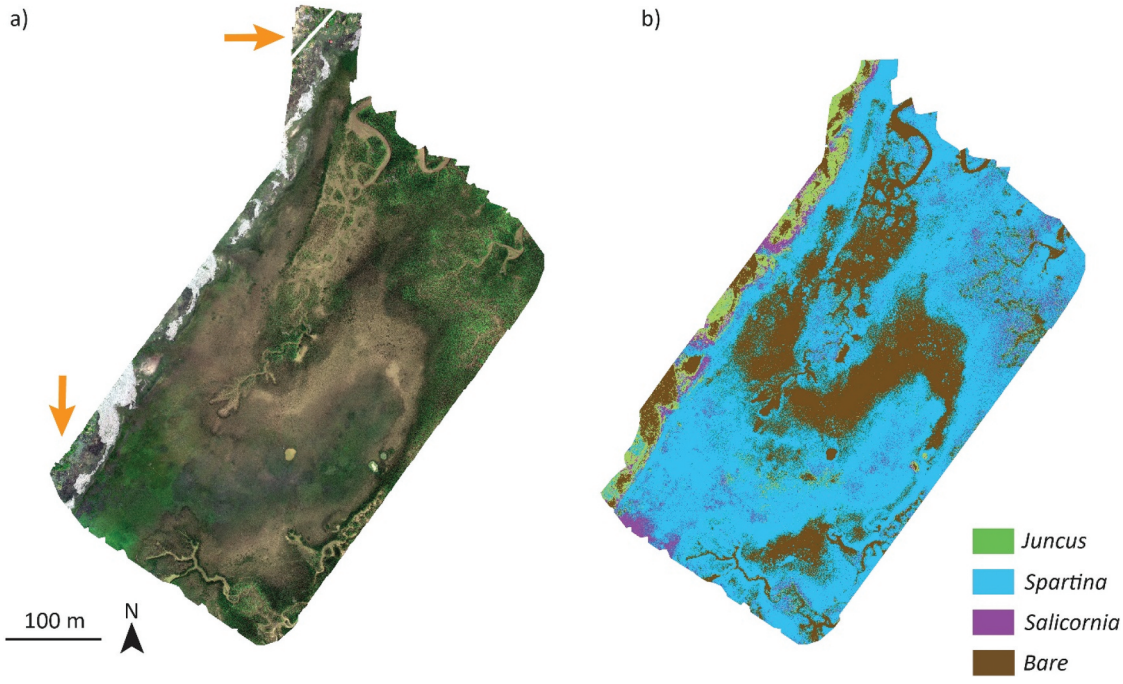

Figure 4. The UAV data (a) and its classification results (b). Panel (a) shows the RGB composition of UAV data. The positions of upland forests and the human-paved road are highlighted by the yellow arrows in panel (a), and excluded from the classification process.

vertical comparison across panels in Figure 5 suggests that, as pixel size increases, the likelihood of encountering pure pixels decreases, which is particularly noticeable for *Juncus* (Figure 5a, **e,** and i) and *Salicornia* (Figure 5b, f and j).

FA estimates within airborne, WV2, and SL2 pixels

The accuracy metrics for the application of RRFR to airborne, WV2, and SL2 data were summarized in Table 2, which demonstrates the robustness of RRFR in unmixing marsh vegetation species. The RRFR achieved acceptable accuracy in unmixing all vegetation species in airborne data pixels, with R^2 >0.40 and RMSE <0.30 in both the test and validation datasets (Figure S4).

The FA estimation accuracy was even higher for the WV2 data, with R^2 >0.70 and RMSE <0.15 in the test dataset. However, the algorithm failed to estimate the FA of *Salicornia* within the validation pixels, as shown by the negative R^2 shown in Table 2. RRFR overestimated the presence of *Salicornia* within pixels with low *Salicornia* presence and underestimated it within pixels with a high *Salicornia* density (Figure S5f).

In SL2 pixels, RRFR demonstrated high robustness in estimating the FA of *Juncus*, *Spartina*, and bare land covers (Figures S6a, c, d), with R^2 >0.70 and RMSE <0.15. Also, in this case, the RRFR had difficulty in estimating the FA of *Salicornia* in SL2 pixels, as indicated by a negative R^2 value (Table 2) and there was no correlation between predicted values and validation data (Figure S6b).

Results for *Salicornia* are poor when the other three classes show good accuracy, especially given that the sum of the RRFR model's estimated results is 100%. This can be attributed to the bias introduced during the rescaling step. If the model slightly overestimates or underestimates the other three dominant classes (soil, *Juncus*, and *Spartina*), it can significantly

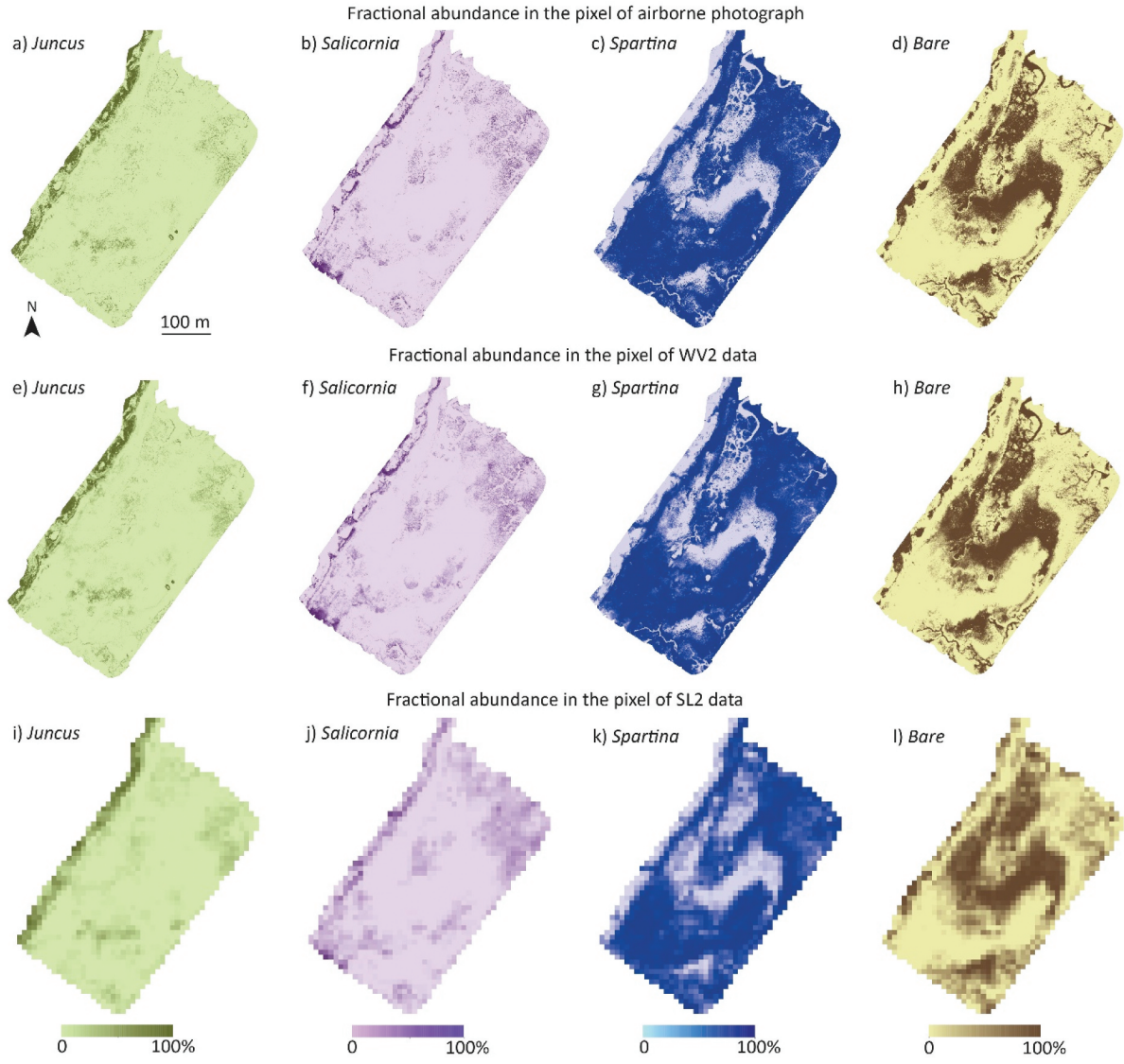

Figure 5. Fractional abundance of each species or bare land cover in the pixels of airborne (a-d), WV2 (e-h), and SL2 data (i-l), which were calculated by the classification result of UAV data (Figure 3b).

Table 2. Accuracy of information for the application of RRFR in estimating FA in airborne, WV2, and SL2 pixels.

	Airborne data				WV2				SL2	
	Test dataset		*Validation dataset*		*Test dataset*		*Validation dataset*		*Test dataset*	
Species	R^2	*RMSE*	R^2	*RMSE*	R^2	*RMSE*	R^2	*RMSE*	R^2	*RMSE*
Juncus	0.797	0.120	0.683	0.136	**0.878**	**0.095**	0.761	0.093	0.738	0.055
Salicornia	0.546	0.160	0.506	0.152	**0.704**	**0.119**	−0.425	0.176	−0.149	0.061
Spartina	0.735	0.206	0.445	0.267	**0.846**	**0.151**	0.575	0.230	0.744	0.148
Bare	0.853	0.160	0.755	0.217	**0.900**	**0.127**	0.927	0.118	0.796	0.135

decrease the accuracy of the estimates for the less frequent species, such as *Salicornia*.

Similar distribution patterns of FA are observed across different spatial resolutions of the data, as depicted in Figure 6, particularly for *Juncus*, *Spartina*, and the bare portions. The distribution of *Salicornia* shows the greatest variability depending on the sensor, confirming the model's poor ability to predict its distribution patterns. It emerged that high FA values of *Juncus* are likely to be observed at the boundaries between marsh and upland tidal forest as well as in the marsh portions to the south, along the main channel of Winyah Bay. High FA values of

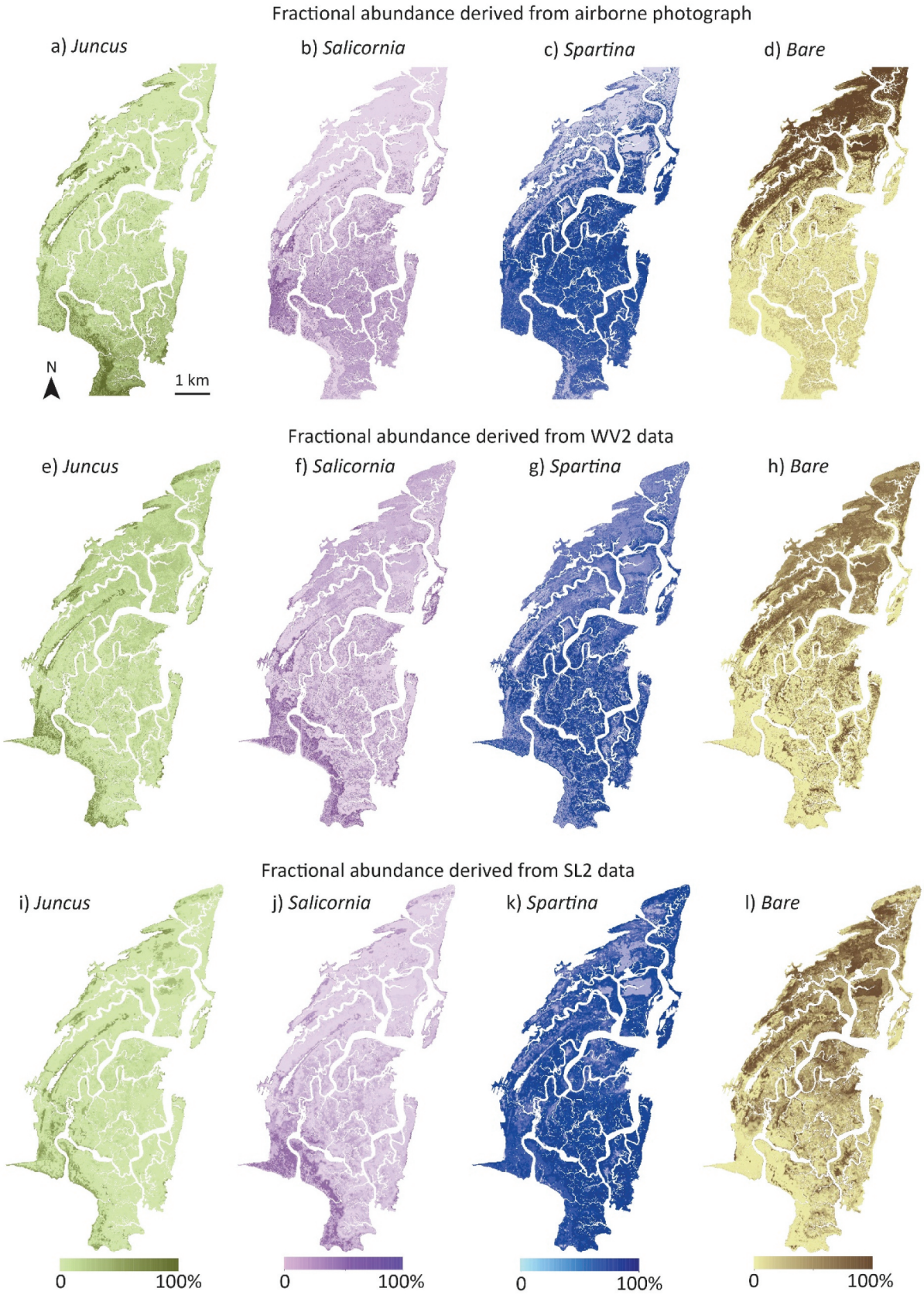

Figure 6. Fractional abundance of each species or bare land cover within the airborne (a-d), WV2 (e-h) and SL2 (i-l) pixels. The scale bar and north arrow in panel (a) apply to all panels; the legends in panel (i-l) apply to each corresponding row, respectively.

Spartina and bare areas tend to occur on marsh platforms in the North Inlet. The presence of *Salicornia*, comparing Figures 6b, f and j, reveals that the FA within WV2 and SL2 is likely overestimated in Winyah Bay. Additionally, extensive areas with high FA of bare surfaces occurred in the region between the marsh upland boundary and North Inlet.

Comparisons between rescaled WV2 FA and SL2 FA

We conducted a comparison between the resampled WV2-derived FA values (Figure S7) and FA derived from the SL2 data (Figure 6i-l). Compared to the WV2 data, SL2 likely underestimated the FA values of *Juncus* and *Salicornia*, as indicated by the slopes of the regression lines for these two species ranging from 0.30 to 0.50 (see Figures 7a, b). In contrast, the FA values of *Spartina* and bare classes derived from WV2 and SL2 are similar, with the slopes of the regression lines for *Spartina* (Figure 7c) and bare classes (Figure 7d) being close to 1 and exhibiting high r^2 values (>0.70).

Discussion

In this study, we demonstrate that the challenges in collecting enough field observations suitable for estimating the FA of various species can be efficiently addressed by simply using a UAV system to acquire (extremely high spatial resolution) multispectral data over a small portion of the marshland. Subsequently, this mapped portion can be used to extract the information required to determine the FA from aerial or satellite-borne data with lower spatial resolutions. Our analyses demonstrate that the RFC hard classification achieves high accuracy in classifying marsh species using multi-spectral UAV data. In addition to the Confusion Matrix and accuracy metrics (Table 1), visual comparisons of the RGB composition of UAV data (Figure 4a) and the classification results

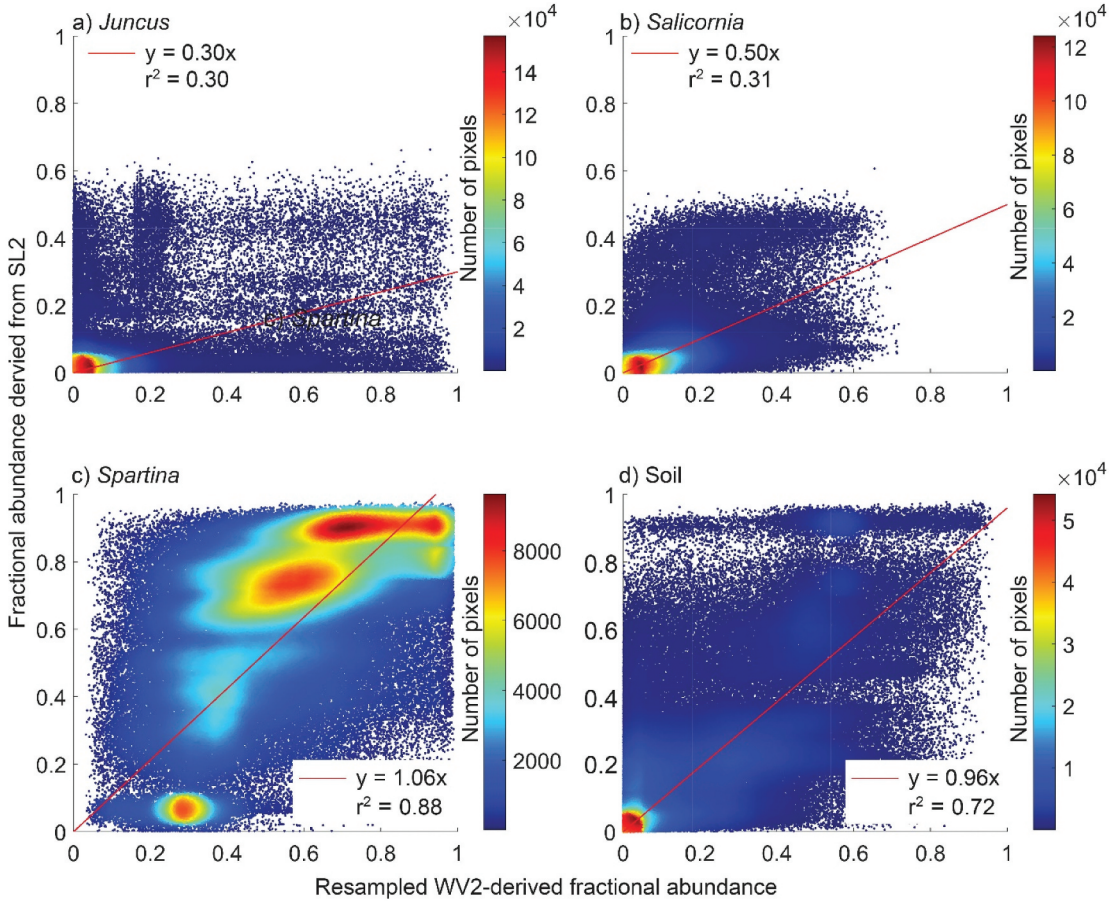

Figure 7. Comparison of resampled fractional abundance derived from WV2 data and fractional abundance derived from SL2 data. The red line and r^2 in each panel represent the result of linear regression and goodness of fit, respectively.

(Figure 4b) indicate accurate classification of vegetated and bare pixels. The size of the area surveyed by the UAV system is crucial for the unmixing process, particularly the presence of large patches of all dominant species of interest within it. Despite RRFR being unable to accurately estimate the FA of less frequent species (*Salicornia*), our analyses indicate that an area of 0.15 km^2 is sufficient to train and validate the unmixing for dominant species (*Juncus* and *Spartina*) and bare areas using airborne photography and WV2 data. We acknowledge that a larger surveyed area would have been desirable for SL2 data, especially if an additional validation dataset can be provided.

The Validation dataset, additional to the Test dataset, proved extremely valuable in confirming or challenging the accuracy of the results, as shown in Table 2. For example, focusing solely on the Test dataset, our analyses indicate that RRFR generally achieved high accuracy in unmixing marsh vegetation species using airborne and WV2 data, as suggested by the generally high R^2 and low RMSE values (Table 2). However, the Validation dataset (Table 2) shows a general decrease in R^2 values for airborne photography, even though the RMSE remains relatively constant, suggesting a general decrease in the method's performance. Similar reductions in accuracy metrics have been observed in previous work mapping freshwater habitats (Berhane et al. 2019). This can be attributed to the fact that the testing datasets are derived from the same patches of the training datasets, while the validation datasets are spatially independent of the training datasets. This highlights that using a spatially independent validation dataset provides a more robust assessment of FA estimation (Berhane et al. 2019). Additionally, for the WV2 data, the Validation R^2 values are quite low for *Salicornia*, suggesting that when predicting FA values at the entire marsh scale, the RRFR fails to estimate the *Salicornia* FA accurately. The failure to retrieve a good estimation of the *Salicornia* FA at a coarser resolution is confirmed by the R^2 value close to 0 from the Test dataset obtained with the SL2 data.

Furthermore, the RRFR appears to overestimate the FA values of *Juncus* and *Salicornia* within SL2 pixels (Figures. 6a, b). We speculate that the sizes of the *Juncus* and *Salicornia* patches within the UAV surveyed area (Figures 2 and 3) were too small compared with the pixel size of SL2. This resulted in a limited number of SL2 pixels with a high abundance of these two species. This is confirmed by Figures 4a, e, and i for *Juncus* and Figures 4b, **f,** and j for *Salicornia*, further hindering the RRFR training. The limited number of WV2 pixels with a high *Salicornia* FA within the UAV area (Figure 5f) is likely the reason for the low accuracy of the *Salicornia* FA estimated from the WV2 pixels. We thus speculate that sufficient training spectral information, extracted from pure or mixed ground-truthing patches, is vital for estimating the FA of target species (Costa, Foody, and Boyd 2017). Further work is needed to examine the performance of RRFR by using more extensive UAV flights that better sample infrequently occurring species in different marsh portions.

The FA maps of vegetation species and bare soil from each sensor in Figure 6 confirm the merits and limits of the method discussed above. The FA of bare soil and *Spartina* appears to be well captured by the RRFR. This confirms that they are predominantly found within the main marsh basin of the North Inlet. However, bare soil may be overestimated in the Winyah Bay area, where marshes have been observed to host-dense vegetation (Li et al. 2020, 2022), especially for the SL2 dataset (comparing Figure 6d, h, and l). The reason for such overestimation can be attributed to the fact that marshes are periodically submerged by the tide, and the presence of water can significantly alter the spectral reflectance (Kearney et al. 2009). As expected, *Juncus* exhibits a preference for marsh landward boundaries and marshes close to Winyah Bay. The *Salicornia* maps retrieved from WV2 (Figure 6f) and SL2 (Figure 6j) are questionable, as they clearly overestimate their presence in the Winyah Bay area when compared with the counterpart map derived from aerial photographs (Figure 6b). Generally, the distribution patterns found in this study align with previous field observations (Allen et al. 2008; Dame and Gardner 1993) and land cover maps (Li et al. 2020, 2022), which can be mainly attributed to spatial variations in salinity and flooding frequency (Pennings, Grant, and Bertness 2005). Marshes adjacent to upland forests, characterized by higher elevations, typically experience lower salinity levels, facilitating the growth of *Juncus*. In contrast, marshes in the central basin have higher salinity due to lower

elevations and limited freshwater input from the uplands and therefore are predominantly occupied by *Spartina*.

Our findings suggest that RRFR can accurately separate *Spartina* and *Juncus* as well as bare soil across various spatial resolutions, while more training and validation datasets are necessary to accurately map the *Salicornia* FA. To the extent of our current knowledge, this study presents the first demonstration of RRFR's robustness in estimating the FA of marsh species. This aligns with its successful performance in mapping vegetation species in other ecosystems. RRFR achieves an accuracy of $0.57 < R^2 < 0.93$ and $0.05 < \text{RMSE} < 0.27$ for dominant species in this study. This accuracy is similar to that reported for forest ecosystems ($0.60 < R^2 < 0.85$ and $0.10 < \text{RMSE} < 0.20$, Immitzer et al. 2018) and coastal habitats ($0.40 < R^2 < 0.63$ and $0.21 < \text{RMSE} < 0.26$, Martínez Prentice et al. 2024). This highlights the potential of RRFR as a valuable tool for mapping and monitoring marsh vegetation, particularly for large-scale applications where traditional field surveys may be impractical.

Nevertheless, we note that the RRFR failed to achieve a good level of performance in the Venice lagoon salt marshes (Yang et al. 2020). The relatively poor performance of RRFR in the Venice lagoon was attributed to a very high level of species intermixing at small spatial scales, and thus high species heterogeneity within a pixel (Yang et al. 2020). This poses the question of determining the limit of RRFR relative to a measure of the degree of species mixing. Additionally, Yang et al. (2020) demonstrated superior performance of Random Forest Soft Classification in such highly mixed systems, which was not found in the North Inlet case. This underscores the importance of selecting the most suitable method based on the specific ecological characteristics and local conditions of the study area.

We also acknowledge that spectral differences exist between wrack and bare soil, which could introduce some inaccuracy in our estimations. However, when comparing the UAV data's RGB composition with the RFC classification results (Figure 4), both wrack and bare areas were consistently classified as bare, suggesting that considering these two types as one individual class did not impact the RFC classification accuracy. Additionally, wrack patches have a relatively short lifespan, often degrading within 3 months (Lynn et al. 2023) and tend to result in vegetation mortality (Pennings and Richards 1998). Given that our WV2 and some of the SL2 scenes used to obtain the SL2 data were acquired at a later time than the UAV data, we assume that most wrack patches were decomposed by the time of satellite image acquisition. Furthermore, previous studies indicate that wrack coverage in marsh environments is generally low (~2%; see Lynn et al. 2023), supporting the assumption that its impact on unmixing accuracy is negligible.

Despite RRFR not excelling when applied to SL2 data, the general spatial distribution of each species derived from RRFR, especially *Spartina* and bare soil, is similar to that obtained from finer resolution data. Therefore, we suggest that it is sufficiently accurate for large-area monitoring. This highlights the potential for utilizing publicly available, though spatially coarse, satellite multi-spectral data (e.g. Planet, Sentinel, and Landsat) to map marsh species distribution by relying on a limited training dataset based on UAV data collection.

This approach can facilitate the analysis and monitoring of marsh vegetation dynamics, encompassing phenomena such as dieback and recovery, alien species invasion, and inter-specific replacement, all of which profoundly influence marsh ecological processes and vulnerability. By reducing the reliance on costly high-spatial resolution multispectral remote sensing data sources (e.g. Belluco et al. 2006; Doughty et al. 2021; Klemas 2011; Sun et al. 2020; Wang et al. 2007; Yang et al. 2020) and repeated labor-intensive field surveys (e.g. Granse, Suchrow, and Jensen 2021; Silvestri, Defina, and Marani 2005; Yang et al. 2023), this approach offers cost-effective and efficient solutions for marsh ecological monitoring and management, which can inform management decisions. Moreover, this approach holds potential implications for estimating marsh vulnerability by using metrics such as areal unvegetated/vegetated marsh ratios (Ganju et al. 2017) and other vulnerability metrics derived from temporal series of vegetation growth conditions (e.g. Scheffer et al. 2009), which can be effectively captured through FA. Such vulnerability assessments can further inform decisions to prioritize conservation efforts, establish early warning systems, and long-term monitoring programs.

Conclusions

Mapping the fractional abundance of marsh plants and bare soil can accurately display species distributions, thus providing critical information on marsh

ecological processes and informing marsh evolution models. Therefore, unmixing vegetation is important for improving the understanding of marsh vulnerability to climate changes and sea level rise.

This study demonstrated that the RFC achieves extremely high accuracy when classifying marsh species based on UAV imagery, underscoring that the use of UAVs can be a cost-effective and efficient method for acquiring the detailed ground truth data necessary for vegetation unmixing across different sensors.

RRFR showed the high level of accuracy when estimating the FA of dominant species (*Spartina* and *Juncus*) and bare soil within the pixels of aerial, WV2, and SL2 data. However, the estimation of FA of *Salicornia*, a minor species within the UAV-acquisition area, in coarser pixels (WV2 and SL2) posed challenges, indicating a need for more UAV data capturing the minor species in various marsh areas. Despite that, the general spatial distribution of FA for each species derived by RRFR can be sufficient to represent vegetation distribution and accurate enough for large-area monitoring.

The high accuracy of RRFR across different spatial resolutions underscores its potential for widespread application in marsh monitoring, particularly with reference to dominant species (*Spartina* and *Juncus*) and bare soil, offering a viable alternative to labor-intensive field surveys and expensive high-resolution aerial photographs and satellite data acquisitions. However, further research is needed to improve the accuracy of FA estimation for less frequently occurring species like *Salicornia*.

By providing detailed information on species distribution and abundance, this approach can support the development of targeted management strategies to address specific threats to marsh ecosystems, such as rising sea levels, invasive species, and nutrient pollution. This approach can facilitate the analysis and monitoring of marsh vegetation dynamics, thereby supporting effective conservation and management practices, which enhance marsh resilience against environmental changes.

Acknowledgments

We are grateful for constructive reviews from anonymous reviewers and the editor, which helped improve this paper. We thank Sofia Avendano, Joshua Matheson, and Rebecca Edgell for their assistance in field observations and UAV imagery collection. We also thank Max Cawley, David Knudsen, Madeline James, Steve Scholle, and Peregrine Bratschi for the discussion on species distribution. This work was supported by the National Science Foundation under Grant No. 2016068, project title: "Coupled Ecological-Geomorphological Response of Coastal Wetlands to Environmental Change." This study was supported within the RETURN Extended Partnership and received funding from the European Union Next-Generation EU (National Recovery and Resilience Plan – NRRP, Mission 4, Component 2, Investment 1.3 – D.D. 1243 2/8/2022, PE0000005). Z.Y. was also supported by Georgia Coastal Ecosystems Long Term Ecological Research project (NSF OCE-1832178).

Author contributions

Z.Y.: Conceptualization, Data curation, Formal analysis, Invesitgation Methodology, Visualization, Writing – original draft, Writing – review and editing. T.B.: Conceptualization, Data curation, Writing – review and editing; C.L.: Conceptualization, Data curation; N.B.: Conceptualization, Data curation; A.D.A.: Conceptualization, Formal analysis, Invesitgation, Methodology, Supervision, Visualization, Writing – review and editing; M.M.: Conceptualization, Data curation, Formal analysis, Funding acquisition, Investigation, Methodology, Supervision, Visualization, Writing – review and editing; B.M.: Conceptualization, Data curation, Formal analysis, Funding acquisition, Investigation, Methodology, Supervision, Visualization, Writing – review and editing; S.S.: Conceptualization, Data curation, Formal analysis, Funding acquisition, Investigation, Methodology, Supervision, Visualization, Writing – original draft, Writing – review and editing.

Data availability statement

The classification results of drone images are available at: https://figshare.com/s/563c24cf1f17aee7c89e. The fractional abundance maps of aerial, WV2, and Sentinel 2 data are available at: https://figshare.com/s/0d7f75fbf5352065b13d., https://figshare.com/s/4f33aa392362c56af7eb., and https://figshare.com/s/b9680afca629b355830a, respectively.

Disclosure statement

No potential conflict of interest was reported by the author(s).

Funding

The work was supported by the National Science Foundation [2016068] and [OCE-1832178] and European Union Next-Generation EU [PE0000005]

ORCID

Zhicheng Yang http://orcid.org/0000-0002-0730-6323

References

Alber, M., E. M. Swenson, S. C. Adamowicz, and I. A. Mendelssohn. 2008. "Salt Marsh Dieback: An Overview of Recent Events in the US." *Estuarine Coastal and Shelf Science* 80 (1): 1–11. https://doi.org/10.1016/j.ecss.2008.08.009.

Allen, D. M., V. Ogburn-Matthews, T. Buck, and E. M. Smith. 2008. "Mesozooplankton Responses to Climate Change and Variability in a Southeastern U.S. Estuary (1981–2003)." *Journal of Coastal Research* 10055:95–110. https://doi.org/10.2112/si55-004.1.

Allen, J. R. L. L. 2000. "Morphodynamics of Holocene Salt Marshes: A Review Sketch from the Atlantic and Southern North Sea Coasts of Europe." *Quaternary Science Reviews* 19 (12): 1155–1231. https://doi.org/10.1016/S0277-3791(99)00034-7.

Barbier, E. B., S. D. Hacker, C. Kennedy, E. W. Koch, A. C. Stier, and B. R. Silliman. 2011. "The Value of Estuarine and Coastal Ecosystem Services." *Ecological Monographs* 81 (2): 169–193. https://doi.org/10.1890/10-1510.1.

Belgiu, M., and L. Drăgu. 2016. "Random Forest in Remote Sensing: A Review of Applications and Future Directions." *Isprs Journal of Photogrammetry & Remote Sensing* 114:24–31. https://doi.org/10.1016/j.isprsjprs.2016.01.011.

Belluco, E., M. Camuffo, S. Ferrari, L. Modenese, S. Silvestri, A. Marani, and M. Marani. 2006. "Mapping Salt-Marsh Vegetation by Multispectral and Hyperspectral Remote Sensing." *Remote Sensing of Environment* 105 (1): 54–67. https://doi.org/10.1016/j.rse.2006.06.006.

Berhane, T. M., H. Costa, C. R. Lane, O. A. Anenkhonov, V. V. Chepinoga, and B. C. Autrey. 2019. "The Influence of Region of Interest Heterogeneity on Classification Accuracy in Wetland Systems." *Remote Sensing* 11 (5): 1–16. https://doi.org/10.3390/rs11050551.

Blum, M. D., and H. H. Roberts. 2009. "Drowning of the Mississippi Delta Due to Insufficient Sediment Supply and Global Sea-Levelrise." *Nature Geoscience* 2 (7): 488–491. https://doi.org/10.1038/ngeo553.

Bouma, T. J., L. A. van Duren, S. Temmerman, T. Claverie, A. Blanco-Garcia, T. Ysebaert, and P. M. J. Herman. 2007. "Spatial Flow and Sedimentation Patterns within Patches of Epibenthic Structures: Combining Field, Flume and Modelling Experiments." *Continental Shelf Research* 27 (8): 1020–1045. https://doi.org/10.1016/j.csr.2005.12.019.

Breiman, L. 2001. "Random Forests." *Machine Learning* 45 (1): 5–32.

Campbell, A., Y. Wang, M. Christiano, and S. Stevens. 2017. "Salt Marsh Monitoring in Jamaica Bay, New York from 2003 to 2013: A Decade of Change from Restoration to Hurricane Sandy." *Remote Sensing* 9 (2): 1–20. https://doi.org/10.3390/rs9020131.

Carniello, L., A. Defina, and L. D'Alpaos. 2009. "Morphological Evolution of the Venice Lagoon: Evidence from the Past and Trend for the Future." *Journal of Geophysical Research: Earth Surface* 114 (F4): 1–10. https://doi.org/10.1029/2008JF001157.

Chai, G., J. Wang, G. Wang, L. Kang, M. Wu, and Z. Wang. 2019. "Estimating Fractional Cover of Non-Photosynthetic Vegetation in a Typical Grassland Area of Northern China Based on Moderate Resolution Imaging Spectroradiometer (MODIS) Image Data." *International Journal of Remote Sensing* 40 (23): 8793–8810. https://doi.org/10.1080/01431161.2019.1620971.

Chai, T., and R. R. Draxler. 2014. "Root Mean Square Error (RMSE) or Mean Absolute Error (MAE)? – Arguments Against Avoiding RMSE in the Literature." *Geoscientific Model Development* 7 (3): 1247–1250. https://doi.org/10.5194/gmd-7-1247-2014.

Cooley, T., G. P. Anderson, G. W. Felde, M. L. Hoke, A. J. Ratkowski, J. H. Chetwynd, J. A. Gardner, et al. 2002. "FLAASH, a MODTRAN4-Based Atmospheric Correction Algorithm, Its Applications and Validation." *Int Geosci Remote Sens Symp* 3:1414–1418. https://doi.org/10.1109/igarss.2002.1026134.

Costa, H., G. M. Foody, and D. S. Boyd. 2017. "Using Mixed Objects in the Training of Object-Based Image Classifications." *Remote Sensing of Environment* 190:188–197. https://doi.org/10.1016/j.rse.2016.12.017.

Dai, W., H. Li, Z. Gong, Z. Zhou, Y. Li, L. Wang, C. Zhang, and H. Pei. 2021. "Self-Organization of Salt Marsh Patches on Mudflats: Field Evidence Using the UAV Technique." *Estuarine Coastal and Shelf Science* 262:107608. https://doi.org/10.1016/j.ecss.2021.107608.

Da Lio, C., A. D'Alpaos, and M. Marani. 2013. "The Secret Gardener: Vegetation and the Emergence of Biogeomorphic Patterns in Tidal Environments." *Philosophical Transactions of the Royal Society A: Mathematical, Physical and Engineering Sciences* 371 (2004): 371. https://doi.org/10.1098/rsta.2012.0367.

D'Alpaos, A., S. Lanzoni, M. Marani, S. Fagherazzi, and A. Rinaldo. 2005. "Tidal Network Ontogeny: Channel Initiation and Early Development." *Journal of Geophysical Research: Earth Surface* 110 (F2): 1–14. https://doi.org/10.1029/2004JF000182.

D'Alpaos, A., S. M. Mudd, and L. Carniello. 2011. "Dynamic Response of Marshes to Perturbations in Suspended Sediment Concentrations and Rates of Relative Sea Level Rise." *Journal of Geophysical Research* 116 (F4): 1–13. https://doi.org/10.1029/2011JF002093.

Dame, R. F., and L. R. Gardner. 1993. "Nutrient Processing and the Development of Tidal Creek Ecosystems." *Marine Chemistry* 43 (1–4): 175–183. https://doi.org/10.1016/0304-4203(93)90223-B.

Deegan, L. A., D. S. Johnson, R. S. Warren, B. J. Peterson, J. W. Fleeger, S. Fagherazzi, and W. M. Wollheim. 2012. "Coastal Eutrophication as a Driver of Salt Marsh Loss." *Nature* 490 (7420): 388–392. https://doi.org/10.1038/nature11533.

Doughty, C. L., R. F. Ambrose, G. S. Okin, K. C. Cavanaugh, M. Disney, and C. De Angelo. 2021. "Characterizing Spatial Variability in Coastal Wetland Biomass Across Multiple Scales Using UAV and Satellite Imagery." *Remote Sensing in Ecology and Conservation* 7 (3): 411–429. https://doi.org/10.1002/rse2.198.

Doughty, C. L., and K. C. Cavanaugh. 2019. "Mapping Coastal Wetland Biomass from High Resolution Unmanned Aerial Vehicle (UAV) Imagery." *Remote Sensing* 11 (5): 11. https://doi.org/10.3390/rs11050540.

European Space Agency. "Sentinel-2 User Handbook." Accessed March 19, 2025. https://sentinel.esa.int/documents/247904/685211/Sentinel-2_User_Handbook.

Finotello, A., A. D'Alpaos, M. Marani, and E. Bertuzzo. 2022. "A Minimalist Model of Salt-Marsh Vegetation Dynamics Driven by Species Competition and Dispersal." *Frontiers in Marine Science* 9:1–23. https://doi.org/10.3389/fmars.2022.866570.

Foody, G. M. 2002. "Status of Land Cover Classification Accuracy Assessment. Remote Sens." *Remote Sensing of Environment* 80 (1): 185–201. https://doi.org/10.1016/S0034-4257(01)00295-4.

Ganju, N. K., B. R. Couvillion, Z. Defne, and K. V. Ackerman. 2022. "Development and Application of Landsat-Based Wetland Vegetation Cover and UnVegetated-Vegetated Marsh Ratio (UVVR) for the Conterminous United States. Estuaries and Coasts." *Estuaries & Coasts* 45 (7): 1861–1878. https://doi.org/10.1007/s12237-022-01081-x.

Ganju, N. K., Z. Defne, M. L. Kirwan, S. Fagherazzi, A. D'Alpaos, and L. Carniello. 2017. "Spatially Integrative Metrics Reveal Hidden Vulnerability of Microtidal Salt Marshes." *Nature Communications* 8 (1): 14156. https://doi.org/10.1038/ncomms14156.

Gates, D. M., H. J. Keegan, J. C. Schleter, and V. R. Weidner. 1965. "Spectral Properties of Plants." *Applied Optics* 4 (1): 11. https://doi.org/10.1364/ao.4.000011.

Granse, D., S. Suchrow, and K. Jensen. 2021. "Long-Term Invasion Dynamics of Spartina Increase Vegetation Diversity and Geomorphological Resistance of Salt Marshes Against Sea Level Rise." *Biological Invasions* 23 (3): 871–883. https://doi.org/10.1007/s10530-020-02408-0.

Horton, B. P., I. Shennan, S. L. Bradley, N. Cahill, M. Kirwan, R. E. Kopp, and T. A. Shaw. 2018. "Predicting Marsh Vulnerability to Sea-Level Rise Using Holocene Relative Sea-Level Data." *Nature Communications* 9 (1): 4–10. https://doi.org/10.1038/s41467-018-05080-0.

Howes, N. C., D. M. FitzGerald, Z. J. Hughes, I. Y. Georgiou, M. A. Kulp, M. D. Miner, J. M. Smith, and J. A. Barras. 2010. "Hurricane-Induced Failure of Low Salinity Wetlands." *Proceedings of the National Academy of Sciences* 107 (32): 14014–14019. https://doi.org/10.1073/pnas.0914582107.

Hughes, A. L. H., A. M. Wilson, and J. T. Morris. 2012. "Hydrologic Variability in a Salt Marsh: Assessing the Links Between Drought and Acute Marsh Dieback." *Estuarine Coastal and Shelf Science* 111:95–106. https://doi.org/10.1016/j.ecss.2012.06.016.

Immitzer, M., S. Böck, K. Einzmann, F. Vuolo, N. Pinnel, A. Wallner, and C. Atzberger. 2018. "Fractional Cover Mapping of Spruce and Pine at 1 ha Resolution Combining Very High and Medium Spatial Resolution Satellite Imagery." *Remote Sensing of Environment* 204:690–703. https://doi.org/10.1016/j.rse.2017.09.031.

Juel, A., G. B. Groom, J. C. Svenning, and R. Ejrnæs. 2015. "Spatial Application of Random Forest Models for Fine-Scale Coastal Vegetation Classification Using Object Based Analysis of Aerial Orthophoto and DEM Data." *International Journal of Applied Earth Observation and Geoinformation* 42:106–114. https://doi.org/10.1016/j.jag.2015.05.008.

Kaplan, G. 2018. "Sentinel-2 Pan Sharpening—Comparative Analysis." The 2nd International Electronic Conference on Remote Sensing, Basel Switzerland: 345. MDPI. https://doi.org/10.3390/ecrs-2-05158.

Kearney, M. S., D. Stutzer, K. Turpie, and J. C. Stevenson. 2009. "The Effects of Tidal Inundation on the Reflectance Characteristics of Coastal Marsh Vegetation." *Journal of Coastal Research* 256:1177–1186. https://doi.org/10.2112/08-1080.1.

Klemas, V. 2011. "Remote Sensing Techniques for Studying Coastal Ecosystems: An Overview." *Journal of Coastal Research* 27:2–17. https://doi.org/10.2112/JCOASTRES-D-10-00103.1.

Kvålseth, T. O. 1985. "Cautionary Note About R2." *American Statistician* 39 (4): 279–285. https://doi.org/10.1080/00031305.1985.10479448.

Lane, C. R., H. Liu, B. C. Autrey, O. A. Anenkhonov, V. V. Chepinoga, and Q. Wu. 2014. "Improved Wetland Classification Using Eight-Band High Resolution Satellite Imagery and a Hybrid Approach." *Remote Sensing* 6 (12): 12187–12216. https://doi.org/10.3390/rs61212187.

Li, H., C. Wang, J. T. Ellis, Y. Cui, G. Miller, and J. T. Morris. 2020. "Identifying Marsh Dieback Events from Landsat Image Series (1998–2018) with an Autoencoder in the NIWB Estuary, South Carolina." *International Journal of Digital Earth* 13 (12): 1467–1483. https://doi.org/10.1080/17538947.2020.1729263.

Li, H., C. Wang, Q. Yu, and E. Smith. 2022. "Spatiotemporal Assessment of Potential Drivers of Salt Marsh Dieback in the North Inlet-Winyah Bay Estuary." In *Journal of Environmental Management*, 114907. 313. South Carolina (1990–2019). https://doi.org/10.1016/j.jenvman.2022.114907.

Lynn, T., M. Alber, J. Shalack, D. R. Mishra, and T. Lynn. 2023. "Utilizing Repeat UAV Imagery to Evaluate the Spatiotemporal Patterns and Environmental Drivers of Wrack in a Coastal Georgia Salt Marsh." *Estuaries & Coasts* 47 (1): 189–200. https://doi.org/10.1007/s12237-023-01265-z.

Marani, M., C. Da Lio, and A. D'Alpaos. 2013. "Vegetation Engineers Marsh Morphology Through Multiple Competing Stable States." *Proceedings of the National Academy of Sciences* 110 (9): 3259–3263. https://doi.org/10.1073/pnas.1218327110.

Marani, M., A. D'Alpaos, S. Lanzoni, L. Carniello, and A. Rinaldo. 2007. "Biologically-Controlled Multiple Equilibria of Tidal

Landforms and the Fate of the Venice Lagoon." *Geophysical Research Letter* 34 (11): 1–5. https://doi.org/10.1029/2007GL030178.

Marani, M., A. D'Alpaos, S. Lanzoni, L. Carniello, and A. Rinaldo. 2010. "The Importance of Being Coupled: Stable States and Catastrophic Shifts in Tidal Biomorphodynamics." *Journal of Geophysical Research: Earth Surface* 115 (F4): 1–15. https://doi.org/10.1029/2009JF001600.

Marani, M., A. D'Alpaos, S. Lanzoni, and M. Santalucia. 2011. "Understanding and Predicting Wave Erosion of Marsh Edges." *Geophysical Research Letter* 38 (21): n/a–n/a. https://doi.org/10.1029/2011GL048995.

Marani, M., T. Zillio, E. Belluco, S. Silvestri, A. Maritan, and R. Freckleton. 2006. "Non-Neutral Vegetation Dynamics." *PLOS ONE* 1 (1): 1. https://doi.org/10.1371/journal.pone.0000078.

Martínez Prentice, R., M. Villoslada, R. D. Ward, T. F. Bergamo, C. B. Joyce, and K. Sepp. 2024. "Synergistic Use of Sentinel-2 and UAV-Derived Data for Plant Fractional Cover Distribution Mapping of Coastal Meadows with Digital Elevation Models." *Biogeosciences* 21 (6): 1411–1431. https://doi.org/10.5194/bg-21-1411-2024.

Moffett, K. B., and S. M. Gorelick. 2013. "Distinguishing Wetland Vegetation and Channel Features with Object-Based Image Segmentation." *International Journal of Remote Sensing* 34 (4): 1332–1354. https://doi.org/10.1080/01431161.2012.718463.

Möller, I., M. Kudella, F. Rupprecht, T. Spencer, M. Paul, B. K. Van Wesenbeeck, G. Wolters, et al. 2014. "Wave Attenuation Over Coastal Salt Marshes Under Storm Surge Conditions." *Nature Geoscience* 7 (10): 727–731. https://doi.org/10.1038/NGEO2251.

Morgan, G. R., C. Wang, M. E. Hodgson, G. R. Morgan, S. R. Schill, C. Wang, M. E. Hodgson, et al. 2022. "Unmanned Aerial Remote Sensing of Coastal Vegetation: A Review." *Annals of GIS* 28 (3): 385–399. https://doi.org/10.1080/19475683.2022.2026476.

Morris, J. T., P. V. Sundareshwar, C. T. Nietch, B. Kjerfve, and D. R. Cahoon. 2002. "Responses of Coastal Wetlands to Rising Sea Level." *Ecology* 83 (10): 2869–2877. https://doi.org/10.1890/0012-9658%282002%29083%5B2869%3AROCWTR%5D2.0.CO%3B2.

Murray, A. B., M. A. F. Knaapen, M. Tal, and M. L. Kirwan. 2008. "Biomorphodynamics: Physical-Biological Feedbacks That Shape Landscapes." *Water Resources Research* 44 (11): 1–18. https://doi.org/10.1029/2007WR006410.

National Oceanic and Atmospheric Administration. "Tides & Currents: Water Levels at Station 8661070." Wilmington, NC: NOAA Center for Operational Oceanographic Products and Services. Accessed March 19, 2025. https://tidesandcurrents.noaa.gov/waterlevels.html?id=8661070.

Oostdijk, M., M. J. Santos, D. Whigham, J. Verhoeven, and S. Silvestri. 2018. "Assessing Rehabilitation of Managed Mangrove Ecosystems Using High Resolution Remote Sensing." *Estuarine Coastal and Shelf Science* 211:238–247. https://doi.org/10.1016/j.ecss.2018.06.020.

Pafumi, E., C. Angiolini, G. Bacaro, E. Fanfarillo, T. Fiaschi, D. Rocchini, S. Sarmati, M. Torresani, H. Feilhauer, and S. Maccherini. 2025. "Fuzzy Approaches Provide Improved Spatial Detection of Coastal Dune EU Habitats." *Ecological Informatics* 86:103059. https://doi.org/10.1016/j.ecoinf.2025.103059.

Pedregosa, F., G. Varoquaux, A. Gramfort, V. Michel, B. Thirion, O. Grisel, M. Blondel, et al. 2011. "Scikit-Learn: Machine Learning in Python." *Journal of Machine Learning Research* 12:2825–2830. https://doi.org/10.1145/2786984.2786995.

Pennings, S. C., M.-B.-B. Grant, and M. D. Bertness. 2005. "Plant Zonation in Low-Latitude Salt Marshes: Disentangling the Roles of Flooding, Salinity and Competition." *The Journal of Ecology* 93 (1): 159–167. https://doi.org/10.1111/j.1365-2745.2004.00959.x.

Pennings, S. C., and C. L. Richards. 1998. "Effects of Wrack Burial in Salt-Stressed Habitats: Batis Maritima in a Southwest Atlantic Salt Marsh." *Ecography (Cop)* 21 (6): 630–638. https://doi.org/10.1111/j.1600-0587.1998.tb00556.x.

Roner, M., A. D'Alpaos, M. Ghinassi, M. Marani, S. Silvestri, E. Franceschinis, and N. Realdon. 2016. "Spatial Variation of Salt-Marsh Organic and Inorganic Deposition and Organic Carbon Accumulation: Inferences from the Venice Lagoon, Italy." *Advances in Water Resources* 93:276–287. https://doi.org/10.1016/j.advwatres.2015.11.011.

Rosenfield, G. H. F.-L. K. 1986. "A Coefficient of Agreement as a Measure of Thematic Classification Accuracy." *Photogrammetric Engineering* 52: 223–227. https://pubs.usgs.gov/publication/70014667.

Scheffer, M., J. Bascompte, W. A. Brock, V. Brovkin, S. R. Carpenter, V. Dakos, H. Held, E. H. Van Nes, M. Rietkerk, and G. Sugihara. 2009. "Early-Warning Signals for Critical Transitions." *Nature* 461 (7260): 53–59. https://doi.org/10.1038/nature08227.

Schwieder, M., P. J. Leitão, S. Suess, C. Senf, and P. Hostert. 2014. "Estimating Fractional Shrub Cover Using Simulated Enmap Data: A Comparison of Three Machine Learning Regression Techniques." *Remote Sensing* 6 (4): 3427–3445. https://doi.org/10.3390/rs6043427.

Silliman, B. R., J. van de Koppel, M. D. Bertness, L. E. Stanton, and I. A. Mendelssohn. 2005. "Drought, Snails, and Large-Scale Die-Off of Southern U.S. Salt Marshes." *Science* 310 (5755): 1803–1806. https://doi.org/10.1126/science.1118229.

Silvestri, S., A. Defina, and M. Marani. 2005. "Tidal Regime, Salinity and Salt Marsh Plant Zonation." *Estuarine Coastal and Shelf Science* 62 (1–2): 119–130. https://doi.org/10.1016/j.ecss.2004.08.010.

Silvestri, S., M. Marani, and A. Marani. 2003. "Hyperspectral Remote Sensing of Salt Marsh Vegetation, Morphology and Soil Topography." *Physics and Chemistry of the Earth, Parts A/B/C* 28 (1–3): 15–25. https://doi.org/10.1016/S1474-7065(03)00004-4.

Sun, L., D. Shao, T. Xie, W. Gao, X. Ma, Z. Ning, and B. Cui. 2020. "How Does Spartina Alterniflora Invade in Salt Marsh in Relation to Tidal Channel Networks? Patterns and Processes." *Remote Sensing* 12 (18): 1–18. https://doi.org/10.3390/RS12182983.

Timm, B. C., and K. McGarigal. 2012. "Fine-Scale Remotely-Sensed Cover Mapping of Coastal Dune and Salt Marsh Ecosystems at Cape Cod National Seashore Using Random Forests." *Remote Sensing of Environment* 127:106–117. https://doi.org/10.1016/j.rse.2012.08.033.

Tognin, D., A. D'Alpaos, M. Marani, and L. Carniello. 2021. "Marsh Resilience to Sea-Level Rise Reduced by Storm-Surge Barriers in the Venice Lagoon." *Nature Geoscience* 14 (12): 906–911. https://doi.org/10.1038/s41561-021-00853-7.

Van Beijma, S., A. Comber, and A. Lamb. 2014. "Random Forest Classification of Salt Marsh Vegetation Habitats Using Quad-Polarimetric Airborne SAR, Elevation and Optical RS Data." *Remote Sensing of Environment* 149:118–129. https://doi.org/10.1016/j.rse.2014.04.010.

Wang, C., M. Menenti, M. P. Stoll, E. Belluco, and M. Marani. 2007. "Mapping Mixed Vegetation Communities in Salt Marshes Using Airborne Spectral Data." *Remote Sensing of Environment* 107 (4): 559–570. https://doi.org/10.1016/j.rse.2006.10.007.

Xu, M., P. Watanachaturaporn, P. K. Varshney, and M. K. Arora. 2005. "Decision Tree Regression for Soft Classification of Remote Sensing Data." *Remote Sensing of Environment* 97 (3): 322–336. https://doi.org/10.1016/j.rse.2005.05.008.

Yang, L., K. Jia, S. Liang, X. Wei, Y. Yao, and X. Zhang. 2017. "A Robust Algorithm for Estimating Surface Fractional Vegetation Cover from Landsat Data." *Remote Sensing* 9 (8): 1–20. https://doi.org/10.3390/rs9080857.

Yang, Z., C. Alexander, and M. Alber. 2024. "The Dynamics of Marsh-Channel Slump Blocks: An Observational Study Using Repeated Drone Imagery." *Biogeosciences* 21 (7): 1757–1772. https://doi.org/10.5194/bg-21-1757-2024.

Yang, Z., A. D'Alpaos, M. Marani, T. Blount, M. Alber, B. Murray, and S. Silvestri. 2025. "Recovery from Drought-Induced Dieback May Lead to Modified Salt Marsh Vegetation Composition." *Limnology & Oceanography*. https://doi.org/10.1002/lno.12795.

Yang, Z., A. D'Alpaos, M. Marani, and S. Silvestri. 2020. "Assessing the Fractional Abundance of Highly Mixed Salt-Marsh Vegetation Using Random Forest Soft Classification." *Remote Sensing* 12 (19): 3224. https://doi.org/10.3390/rs12193224.

Yang, Z., D. Tognin, A. Finotello, E. Belluco, A. Puppin, S. Silvestri, M. Marani, and A. D'Alpaos. 2023. "Long-Term Monitoring of Coupled Vegetation and Elevation Changes in Response to Sea Level Rise in a Microtidal Salt Marsh." *Journal of Geophysical Research Biogeosciences* 128 (6): 1–17. https://doi.org/10.1029/2023JG007405.

Yuan, X. 2009. "Quality Assessment for GPS-Supported Bundle Block Adjustment Based on Aerial Digital Frame Imagery." *Photogrammetric Record* 24 (126): 139–156. https://doi.org/10.1111/j.1477-9730.2009.00527.x.

Zhou, Z., Y. Yang, and B. Chen. 2018. "Estimating Spartina Alterniflora Fractional Vegetation Cover and Aboveground Biomass in a Coastal Wetland Using SPOT6 Satellite and UAV Data." *Aquatic Botany* 144:38–45. https://doi.org/10.1016/j.aquabot.2017.10.004.

Zong, L., and H. Nepf. 2010. "Flow and Deposition in and Around a Finite Patch of Vegetation." *Geomorphology* 116 (3–4): 363–372. https://doi.org/10.1016/j.geomorph.2009.11.020.